# *De Novo* and Inherited Variants in *GBF1* are Associated with Axonal Neuropathy Caused by Golgi Fragmentation

Natalia Mendoza-Ferreira,[1,10] Mert Karakaya,[1,10] Nur Cengiz,[1] Danique Beijer,[2,3] Karlla W. Brigatti,[4] Claudia Gonzaga-Jauregui,[5] Nico Fuhrmann,[1] Irmgard Hölker,[1] Maximilian P. Thelen,[1] Sebastian Zetzsche,[1] Roman Rombo,[1] Erik G. Puffenberger,[4] Peter De Jonghe,[2,3,6] Tine Deconinck,[2,3] Stephan Zuchner,[7] Kevin A. Strauss,[5] Vincent Carson,[4] Bertold Schrank,[8] Gilbert Wunderlich,[9] Jonathan Baets,[2,3,6] and Brunhilde Wirth[1,11,*]

## Summary

Distal hereditary motor neuropathies (HMNs) and axonal Charcot-Marie-Tooth neuropathy (CMT2) are clinically and genetically heterogeneous diseases characterized primarily by motor neuron degeneration and distal weakness. The genetic cause for about half of the individuals affected by HMN/CMT2 remains unknown. Here, we report the identification of pathogenic variants in *GBF1* (Golgi brefeldin A-resistant guanine nucleotide exchange factor 1) in four unrelated families with individuals affected by sporadic or dominant HMN/CMT2. Genomic sequencing analyses in seven affected individuals uncovered four distinct heterozygous *GBF1* variants, two of which occurred *de novo*. Other known HMN/CMT2-implicated genes were excluded. Affected individuals show HMN/CMT2 with slowly progressive distal muscle weakness and musculoskeletal deformities. Electrophysiological studies confirmed axonal damage with chronic neurogenic changes. Three individuals had additional distal sensory loss. *GBF1* encodes a guanine-nucleotide exchange factor that facilitates the activation of members of the ARF (ADP-ribosylation factor) family of small GTPases. GBF1 is mainly involved in the formation of coatomer protein complex (COPI) vesicles, maintenance and function of the Golgi apparatus, and mitochondria migration and positioning. We demonstrate that GBF1 is present in mouse spinal cord and muscle tissues and is particularly abundant in neuropathologically relevant sites, such as the motor neuron and the growth cone. Consistent with the described role of GBF1 in Golgi function and maintenance, we observed marked increase in Golgi fragmentation in primary fibroblasts derived from all affected individuals in this study. Our results not only reinforce the existing link between Golgi fragmentation and neurodegeneration but also demonstrate that pathogenic variants in *GBF1* are associated with HMN/CMT2.

Hereditary axonal neuropathies are a heterogenous group of disorders characterized by normal or moderately reduced nerve conduction velocities.[1] Classically, they are classified into two subgroups depending on the affected fiber type. The distal hereditary motor neuropathies (HMNs) are characterized by pure motor neuropathy, whereas the axonal Charcot-Marie-Tooth neuropathy (CMT2) have both motor and sensory involvement.[1] The cardinal phenotype of these entities is a length-dependent motor neuropathy that predominantly affects the distal foot and peroneal muscles and results in foot abnormalities or deformities and gait disturbance. Clinically, HMNs/CMT2 present with extreme heterogeneity in terms of onset, clinical course, associated neurological features (i.e., sensory or cerebellar involvement), and other co-presenting signs, including seizures, fractures, and respiratory distress, among others.[2–4] This variability not only results in complex phenotypic categorizations but also in diagnostic challenges and potential misinterpretation of genetic findings.

The integration of next-generation sequencing (NGS) technologies into routine genetic diagnostics and the ensuing yield of novel disease genes has greatly expanded the number of loci associated with axonal neuropathies. Notwithstanding that, a successful genetic diagnosis is possible only in about half of the individuals with HMN/CMT2.[5,6]

Variants in more than 60 genes have been associated with autosomal-dominant forms of HMN or CMT2, which are phenotypically very similar (see "Muscle Gene Table" and "Inherited Neuropathy Variant Browser" in Web Resources). These genes, although functionally heterogeneous, have revealed common molecular mechanisms underlying the pathology of dominant HMNs, such as protein misfolding and aggregation,[7–9] disrupted axonal transport,[9–12] and mitochondria dysfunction.[13–15] Over the past years, we, as well as others, have identified heterozygous variants in BICD cargo adaptor 2, also known as bicaudal D homolog 2 (*Drosophila*) (*BICD2* [MIM: 609797]),

[1]Institute of Human Genetics, Center for Molecular Medicine Cologne, Center for Rare Diseases Cologne, and Institute for Genetics, University of Cologne, 50931 Cologne, Germany; [2]Translational Neurosciences, Faculty of Medicine, University of Antwerp, B-2610 Wilrijk, Belgium; [3]Laboratory of Neuromuscular Pathology, Institute Born-Bunge, University of Antwerp, B-2610 Wilrijk, Belgium; [4]Clinic for Special Children, Strasburg, PA 17579, USA; [5]Regeneron Genetics Center, Regeneron Pharmaceuticals Inc., Tarrytown, NY 10591, USA; [6]Neuromuscular Reference Centre, Department of Neurology, Antwerpen University Hospital, B-2650 Edegem, Belgium; [7]Dr. John T. Macdonald Foundation Department of Human Genetics and Hussman Institute for Human Genomics, Miller School of Medicine, University of Miami, Miami, 33136 FL, USA; [8]DKD Helios Klinik, Department of Neurology, 65191 Wiesbaden, Germany; [9]Department of Neurology and Center for Rare Diseases, University Hospital Cologne, 50931 Cologne, Germany
[10]These authors contributed equally
[11]Twitter: @brunhildewirth
*Correspondence: brunhilde.wirth@uk-koeln.de
https://doi.org/10.1016/j.ajhg.2020.08.018.

associated with dominantly inherited spinal muscular atrophy, lower extremity predominant 2A and 2B (SMA-LED2A/2B [MIM: 615290 and 618291]).[16–20] Precisely, pathogenic variants in *BICD2*, an important golgin and cargo adaptor protein, cause a severe Golgi fragmentation phenotype in primary fibroblasts, increased microtubule stability leading to axonal growth and transport defects in cultured motor neurons, neuromuscular junction (NMJ) development, and locomotor impairment in mutant flies.[21,22]

Here, we report heterozygous variants in Golgi-specific brefeldin A-resistance guanine nucleotide exchange factor 1 (*GBF1* [MIM: 603698]) as being associated with an overlapping phenotype of HMN and CMT2. Our functional data demonstrate that GBF1 is present in neuronal tissues and cells relevant for the motor neuron (MN) pathology. Moreover, *GBF1* variants, similar to *BICD2* variants, lead to a markedly increased Golgi fragmentation phenotype, which was observed, invariably, in all the analyzed probands-derived fibroblasts.

We describe seven individuals carrying *de novo* or autosomal-dominantly inherited variants in *GBF1* leading to a slowly progressive HMN/CMT2; the individuals are from four unrelated families (Figure 1A and Table 1). Informed consent from each studied subject was obtained by each institution (details are given in the Supplemental Material and Methods), and the entire study was conducted under the ethical approval of the University of Cologne (reference number: 13-022).

Proband 1 (family 1, Figure 1A) presented with an HMN. The onset was at 57 years of age and included slowly progressive asymmetric distal muscle weakness predominantly in lower extremities. Parents were reportedly clinically unaffected. Examination of the affected individual at 68 years of age revealed bilateral foot drop, steppage gait, and an asymmetric wasting of the anterior compartment muscles in distal legs (right>left) (Figure 2A). Ankle jerk reflexes were absent. Tibial motor nerve conduction studies revealed normal amplitudes (12 mV), whereas the distal peroneal compound muscle action potential (CMAP) amplitudes were severely reduced (0.1mV on the right side and 0.9 mV on the left) but better preserved when recorded from the anterior tibial muscles (4.9 mV on the right and 12 mV on the left). The sural sensory nerve action potential (SNAP) was also normal (22 μV). Electromyography (EMG) showed spontaneous activity in the lower leg muscles only with chronic neurogenic changes in both the anterior tibial, medial gastrocnemius, and the dorsal interosseous muscle 1 (IOD1). Magnetic resonance imaging (MRI) of the lumbar spine revealed moderate spinal stenosis at the L3-L4 level but no evidence of compressive radiculopathies. MRI of the distal lower extremities revealed asymmetric hyperintensities of the anterior and posterior compartment of the right lower leg, suggesting partial fatty transformation of the affected muscles with much lesser involvement of the left lower leg muscles (Figure 2A).

As part of the NeurOmics consortium, an NGS-based gene panel excluded known mutations in genes implicated in lower motor neuron diseases. Subsequently, a trio-based whole-genome sequencing (trio-WGS) was carried out as previously described[23] via Illumina's TruSeq PCR-free sample preparation kit and run on the Illumina HiSeqX sequencer. The raw sequences were aligned with the Burrows-Wheeler Alignment tool (BWA) (v.0.7.10), duplicates were marked and removed with Picard, and indels were aligned with GATKLite v.2.3.9.

Following the prioritization of variants by allele frequency, conservation, and predicted effect on protein function, a heterozygous *de novo* missense variant in exon 28 (GenBank: NM_004193.3; c.3410C>T [p.Ala1137Val]) was identified in *GBF1* in the affected individual (Figure 1A and Table 1). The variant was absent from our in-house database composed of 3,550 sequenced samples (RD-Connect's integrated platform for rare diseases) but present in the heterozygous state with a minor allele frequency of 2 in 282,866 (MAF = $7 \times 10^{-6}$) in two individuals of African ancestry in gnomAD v.2.1.1. Although the presence of the identified variant in a population database such as gnomAD was controversial and challenging for variant interpretation, we decided to not exclude it and consider it as a plausible candidate because of (1) its *de novo* occurrence in an affected individual without a family history of the disease and (2) the rarity of this variant's being plausible for a mild and adult late-onset phenotype with symptoms starting at 56 years of age in the individual, whereas the ages of the identified individuals in gnomAD were reported as being between 50–55 years.

Proband 2 (III.3), who is currently a 58-year-old female, from family 2, showed progressive weakness in distal extremity muscles. She was first evaluated for her disease at the age of 26 years upon the diagnosis of CMT2 in her aunt. In her family, there were in total five affected individuals from three consecutive generations (Figure 1A). On examination, she showed a steppage gait and walking on heels was not possible. She developed pes cavus and a hammertoe deformity, bilaterally. Nerve conduction studies (NCSs) revealed a clear axonal sensorimotor involvement, and EMG revealed chronic neurogenic changes (Table 1). Exome sequencing (ES) of the index individual was performed within the GENESIS (GEM.app) platform collaboration as previously described.[24] ES identified a heterozygous variant in exon 33 of *GBF1* (GenBank: NM_004193.3; c.4382G>A [p.Arg1461Gln]). The variant was absent from gnomAD and the GENESIS platform of 10,477 individuals, 1,396 of whom presented with CMT and 108 of whom presented with HMN. Sanger sequencing and segregation analyses in the available family members unveiled the same pathogenic variant in two other affected individuals, II.5 and IV.2 (Figure 1A). As expected from these data, the father (III.1) of the affected daughter IV.2 also carries the same variant; he was evaluated at the time of ES in the proband and only had mild complaints of calf muscle cramps in the absence of gait disturbance. Upon

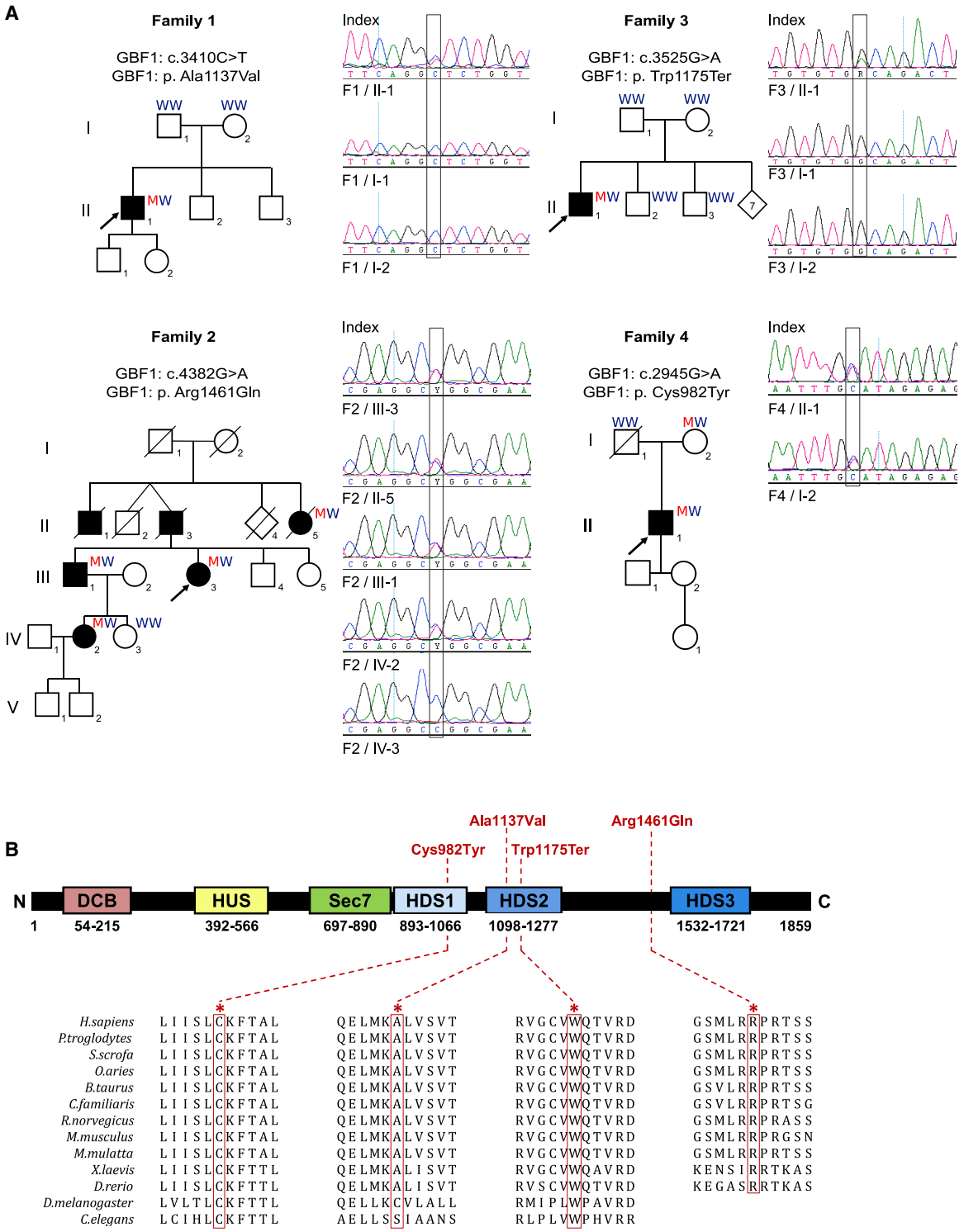


**Figure 1. Pedigrees of the Four Families Affected by *GBF1* Variants, Chromatograms of These Variants, GBF1 Functional Domains, Identified Mutations, and Residues Conservation**

(A) Pedigrees of families 1–4 and Sanger chromatograms of the identified *GBF1* variants. *GBF1* variants are marked in rectangles.

(B) Schematic representation of GBF1 (1,859 amino acids) showing the DCB, HUS, Sec7, and HDS1–3 domains. GBF1 mutations identified in this study as well as their location are marked in red. Protein sequence alignments of GBF1 orthologues are given for each mutated residue. All residues are highly conserved among species. DCB, dimerization and cyclophilin-binding; HUS, homology upstream of Sec7; HDS, homology downstream of Sec7.

**Table 1. Clinical Features of Affected Probands Carrying *GBF1* Variants**

| Family | 1 | 2 | | | | 3 | 4 |
|---|---|---|---|---|---|---|---|
| **Proband** | **II.1** | **III.3** | **II.5** | **III.1** | **IV.2** | **II.1** | **II.1** |
| **Sex/age (years)** | male/73 | female/58 | female/died at 85 years | male/62 | female/39 | male/40 | male/54 |
| **Ethnicity** | German | Belgian | Belgian | Belgian | Belgian | Old Order Amish | German |
| **Genotype** | | | | | | | |
| **Genomic (hg38)** | 10:102370385C>T | 10:102377031G>A | | | | 10:102370728G>A | 10:102368807G>A |
| **Nucleotide** | c.3410C>T | c.4382G>A | | | | c.3525G>A | c.2945G>A |
| **Protein change** | p.Ala1137Val | p.Arg1461Gln | | | | p.Trp1175Ter | p.Cys982Tyr |
| **CADD** | 25.6 | 23.3 | | | | 39 | 31 |
| **Inheritance** | *de novo* | dominant | | | | *de novo* | dominant |
| **Phenotype** | | | | | | | |
| **Age at onset** | 57 years | 24 years | 52 years | 58 years | 33 years | childhood | 50 years |
| **First symptoms** | difficulty walking | difficulty walking | hand weakness, difficulty walking | calf cramps, foot deformities | frequent falls, ankle distortions | delayed motor milestones | difficulty walking |
| **Clinical picture** | distal HMN | CMT2 | CMT2 | CMT2 | CMT2 | CMT2 | distal HMN/SMA peroneal type |
| **ULs—motor** | no | no | mild hand muscle weakness | no | no | hand muscle weakness with bilateral thenar atrophy | slight weakness (score 4/5) in hand and finger muscles |
| **LLs—motor** | foot drop, impaired toe and heel walking R>L | impaired heel walking, pes cavus and hammer toe deformity | mild distal muscle weakness | no | no | foot drop, thin lower extremities, pes cavus deformity | foot drop, weak toe extensors, thin lower extremities, sharp shin sign, pes cavus deformity |
| **ULs—sensory** | normal | N/A | mild hypoesthesia | normal | reduced touch and vibration sense | normal | normal |
| **LLs—sensory** | normal | N/A | mildly reduced vibration sense | normal | reduced touch and vibration sense | numbness in feet, reduced proprioception | numbness in feet |
| **ULs—reflexes** | normal | N/A | absent biceps reflex | normal | normal | reduced biceps, triceps, and brachioradialis reflex | normal |
| **LLs—reflexes** | normal patella reflex, absent ankle jerk reflex | N/A | absent patella (right only) and ankle jerk reflex | normal | absent ankle jerk reflex | brisk patella reflex, absent ankle jerk reflex | brisk patella reflex, absent ankle jerk reflex |
| **Bulbar/vocal** | normal | normal | normal | normal | normal | mild dysarthria | normal |
| **Overall maximal function** | independent ambulation | independent ambulation | independent ambulation | independent ambulation | independent ambulation | independent ambulation | independent ambulation |

(*Continued on next page*)

**Table 1.** ***Continued***

| Family | 1 | 2 | | | | 3 | 4 |
|---|---|---|---|---|---|---|---|
| **Proband** | **II.1** | **III.3** | **II.5** | **III.1** | **IV.2** | **II.1** | **II.1** |
| **Walking aids** | right foot orthosis | no | no | no | no | cane and orthotic inserts | no |
| **EMG** | spontaneous activity in LL with chronic neurogenic changes | chronic neurogenic changes | chronic neurogenic changes | chronic neurogenic changes | normal | chronic neurogenic changes | spontaneous activity in LL with chronic neurogenic changes |
| **NCSs—motor** | axonal involvement | axonal involvement | axonal involvement | axonal involvement | normal UL, mild axonal involvement in LL | axonal involvement | axonal involvement |
| **NCSs—sensory** | normal | axonal involvement | axonal involvement | axonal in UL, reduced velocity in LL (33 m/s) | normal | axonal involvement | normal |
| **MRI muscle** | fatty degeneration of lower extremity muscles, predominantly on the right | N/A | N/A | N/A | N/A | N/A | no |
| **MRI spinal cord** | degenerative changes at lumbar spine, moderate spinal canal stenosis at L3/4 | N/A | N/A | N/A | N/A | normal cervical spine | degenerative changes and moderate spinal stenosis at the thoracolumbar junction |

ULs, upper limbs; LLs, lower limbs; EMG, electromyography; NCSs, nerve conduction studies; MRI, magnetic resonance imaging.

examination, he exhibited foot deformities, and electrophysiological evaluation revealed an axonal neuropathy. This suggests a marked variability in clinical severity within this family.

Proband 3 (II.1) from family 3 (Figure 1A, Table 1) is a 40-year-old male and the only affected individual in a ten-sibling Amish family. Reportedly, he had a mild motor developmental delay thought to be due to a premature birth at 32 weeks. He walked at 18–24 months of age and was always seemingly clumsy as a child. He has had a slowly progressive phenotype. At the age of approximately 30 years, symmetric distal muscle weakness developed leading to thin lower extremities and a high steppage gait, compensatory hip flexion, foot drop, bilateral thenar atrophy, and a pes cavus deformity (Figure 2B). On examination, toe plantar flexion and dorsiflexion were absent (Medical Research Council [MRC] grade 0) and muscle strength in the hand and forearm muscles was reduced (wrist flexion/extension 4/5). He also exhibited mild dysarthria, distal sensory loss in lower extremities, decreased vibratory sense in the right foot (intact on left), and decreased proprioception of the great toes bilaterally, though it was intact in the ankles. Reflexes were 2/4 in biceps, triceps, and brachioradialis bilaterally. Deep tendon reflexes were 3/4 in quadriceps bilaterally and 0/4 in ankles. EMG showed chronic denervation on the right L3-L5 and C5-C6 segments, and tibial and peroneal motor nerve conduction studies showed absent compound muscle action potentials. MRI of the brain revealed minor deep white matter change consistent with periventricular leukomalacia from prematurity. We performed family ES of the proband, both unaffected parents, and two unaffected siblings as previously reported.[25] Genomic DNA was sheared and prepared for exome capture with a custom reagent kit from Kapa Biosystems. Samples were captured with the NimbleGen VCRome 2.1 exome target design and sequenced with 75 bp paired-end sequencing on an Illumina HiSeq 2500 with v4 chemistry. Sequence reads were mapped and aligned to the human genome reference assembly via BWA-mem. Variants and genotypes were called with GATK's HaplotypeCaller. Family-based analysis of the exome data identified a heterozygous *de novo* variant causing an early stop codon in exon 29 of *GBF1* (GenBank: NM_004193.3; c.3525G>A [p.Trp1175Ter]) in the proband. The variant affects a highly conserved residue, and it is absent from population variant databases, including our internal database and gnomAD. This collaboration has been initiated via GeneMatcher.[26]

The fourth proband of family 4 (Figure 1A, Table 1) was a 54-year-old male with a clinical manifestation suggestive of HMN or spinal muscular atrophy (SMA) of peroneal type. At 50 years of age, his symptoms started with gait problems (steppage gait) and distal leg muscle weakness beginning on the right side. On examination, he had weak foot and toe extensors (1/5) presenting with foot drop. There was prominent atrophy of the tibialis anterior muscle causing a prominent appearance of the tibia (shin sign), whereas the dorsal leg muscles were only slightly affected (Figure 2C). He also exhibited mild weakness (4/5) in hand and finger muscles. Deep tendon reflexes were slightly elevated, but the Achilles tendon reflex was absent. Bilateral numbness of feet was reported. NCSs were unremarkable, except for the severely reduced CMAP of the peroneal nerve (0.6 mV on the right and 1.0 mV on the left side). EMG showed fibrillation potentials and positive sharp waves in the anterior tibial muscle on both sides. Chronic neurogenic changes could be observed in the anterior tibial, medial gastrocnemius, rectus femoris, and dorsal interosseous muscle 1 muscles bilaterally. MRI of the spine revealed degenerative changes with moderate spinal stenosis at the thoracolumbar junction. Because we had already included *GBF1* in our diagnostic neuromuscular disease panel, we readily identified a rare heterozygous variant in exon 23 of *GBF1* (GenBank: NM_004193.3; c.2945G>A [p.Cys982Tyr]) in this individual in the routine diagnostic setting. In order to exclude other putative variants in all coding exons of the entire genome, we subsequently performed ES. Analysis of the ES data revealed no other putative variants that could explain the phenotype of this individual. The variant was not present in gnomAD nor in our in-house exome database. Interestingly, the variant was inherited from the putatively unaffected mother who had no neuromuscular complaints at the age of 73 years. However, as we were unable to perform any electrophysiological tests in the mother, a subclinical phenotype with a minor pathology could not be excluded.

*GBF1* (6,403 bp) has a single large transcript of 6.4 kb (GenBank: NM_004193) that encodes 1,859 amino acids. It is relatively intolerant to missense variation, having a positive *Z* score of 2.41 (observed/expected ratio: 0.79, gnomAD v.2.1.1, accessed May 2020).

Of note, during routine splicing analyses (Human Splicing Finder 3.1), the variants c.3410C>T and c.4382G>A were predicted to potentially alter splicing by generating an exonic splicing silencer (ESS) or an exonic splicing enhancer (ESE), respectively. To test whether these two variants could alter *GBF1* transcripts processing, we isolated RNA from cultured fibroblasts from the two probands and controls and performed RT-PCR by using primers flanking exons 27 (c.3410C>T) and 32 (c.4382G>A). In both cases, the generated PCR products corresponded only to full-length transcripts (346 bp for c.3410C>T and 387 bp for c.4382G>A) and excluded the possibility of splicing defects associated with the aforementioned *GBF1* variants (Figure S1 and Supplemental Material and Methods).

*GBF1* encodes a guanine-nucleotide exchange factor (GEF) of the Sec7 domain family that facilitates the GDP-to-GTP exchange for members of the ARF family of small GTPases. The activation of ARF proteins is crucial for the spatial-temporal regulation of membrane dynamics and cell organization.[27,28] The main substrates of GBF1 are the evolutionary conserved class I ARF proteins (*ARF1* [MIM: 103180], *ARF3* [MIM: 103190], and *ARF4* [MIM: 601177]).[27] Residing at the Golgi membrane, the ARF1-GBF1 complex is well known for its important role in the

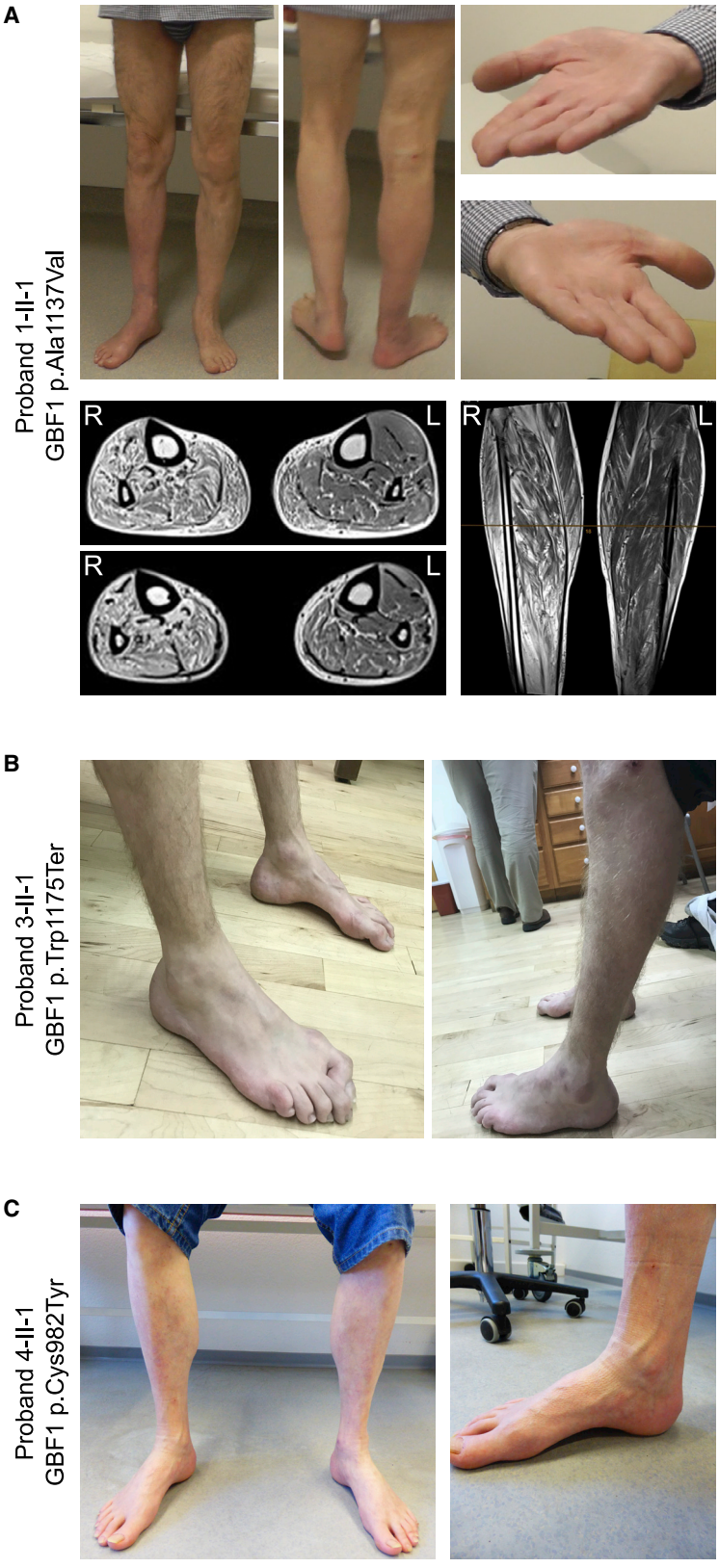


**Figure 2. Clinical Characteristics of the Affected Individuals**

(A) Atrophy of the distal leg muscles and mild atrophy of hand, thenar, and hypothenar muscles of proband 1 (F1/II-1). MRI sections of lower extremities exhibit partial fatty transformation of the entire musculature of the right lower leg and to a lesser degree of the posterior compartment of left lower leg.

(B) Bilateral distal leg and foot muscle atrophy and pes cavus deformity in proband 3 (F3/II-1).

(C) Bilateral atrophy of distal leg muscles prominent in the anterior compartment and pes cavus deformity of the right foot of proband 4 (F4/II-1).

formation of the coatomer protein complex I (COPI) vesicles and the maintenance of the structure and function of the Golgi apparatus (GA).[29–33] Nonetheless in the last years, new and unexpected roles and cellular localizations have been attributed to GBF1 (jointly or independently of ARF1); these include lipid droplet metabolism,[34] mitochondrial function and positioning,[35,36] Clathrin-independent endocytosis,[37,38] and viral/pathogen infection (including corona viruses) and replication processes.[39–43]

The domain architecture of GBF1 includes six partially characterized but highly conserved functional domains. The first two domains of the protein, namely the N-terminal DCB (dimerization and cyclophilin binding) and the HUS (homology upstream of Sec7) domains, regulate the oligomeric state of GBF1.[44,45] The central Sec7 domain catalyzes the GDP/GTP exchange on ARF proteins and thereby their functional activation.[46–48] The C-terminal region of GBF1 is crucial for GBF1 recruitment to the membrane.[40] This region includes three HDS (homology downstream of the Sec7; HDS1–3) domains, of which HDS1 and HDS2 are necessary for GBF1 targeting to the GA because the deletion of these domains, alone or together, inhibits the targeting of the protein to Golgi membranes *in vivo*.[34,49–51] Interestingly, the GBF1 pathogenic variants identified in this study occur in conserved residues that lie in the HDS1 and HDS2 domains of the protein exclusively (Figure 1B). The *in silico* combined annotation-dependent depletion (CADD) prediction scores were high for each variant (Table 1).

Several *in vitro* and *in vivo* studies have revealed important functions of GBF1 in development, physiology, and disease. Reduced GBF1 levels in cultured cells have been associated with loss of GA integrity, COPI dispersal, compromise of the intracellular traffic, and cell death.[32,52,53] Nevertheless, it is important to highlight that tight regulation of GBF1 degradation is necessary for the physiological processes of post-mitotic GA re-assembly and cytokinesis completion.[54] Moreover, GBF1 regulates mitochondrial dynamics because the blocking of GBF1 activity leads to defects in mitochondrial morphology, positioning, and migration.[36]

Loss of function of *arf-1* or *gbf*-1, the ARF1 and GBF1 orthologues in *C. elegans*, cause mitochondrial disorganization, hyperconnectivity, and reduced respiratory activity. Hence, *gbf-1*-depleted worms exhibit a severe reduction in muscle performance and developmental arrest.[35] In vertebrates, the effect of Gbf1 depletion has been documented only in zebrafish. A zebrafish mutant line (*tsu3994*) carrying the loss-of-function Gbf1 mutation Leu1246Arg in the HSD2 domain of the protein exhibits vascular collapse and prominent intracerebral and trunk hemorrhage.[53]

In humans, GBF1 is a ubiquitously abundant protein,[55] however little information exists about its levels in neuronal tissues and specific neuronal populations. Thus, our first step was to confirm the presence of GBF1 in tissues and cells relevant for the HMN/CMT2 phenotype, namely in the spinal cord, brain, and muscle tissues and in MNs.

To analyze the specific localization of GBF1 in primary murine MNs, these were isolated from embryonic day 13.5 (E13.5)-old wild-type (WT) embryos, grown in culture for 7 days, and stained with a GBF1-specific antibody. For the selective visualization of MNs, cells were stained with antibodies against choline acetyltransferase (ChAT), which is routinely used as a marker of cholinergic MNs, and the neuronal-specific microtubule protein tau (Table S1 and Supplemental Material and Methods). Staining showed positive GBF1 signals throughout the whole MN and a particularly high abundance in the soma, and particularly in the GA region and the growth cone tip, where it is present in vesicle-like structures (Figures 3A–3C).

To shed some light onto the developmental requirements of GBF1, we analyzed protein levels during *in vitro* MN differentiation, i.e., days of *in vitro* culture (DIV) 4, 12, and 20, in WT embryonic MNs via immunoblot. Cells were supplemented with specific growth factors in order to promote neuronal differentiation *in vitro* (Supplemental Material and Methods). We observed a steady decrease in levels of GBF1 and increase of ARF1—a main GBF1-interacting partner—during the 20 days of neuronal differentiation (Figure 3D). Moreover, we confirmed GBF1 presence in total protein lysates from the brain, spinal cord, and muscle (gastrocnemius) isolated from WT mice at different postnatal stages (Figure S2). Both GBF1 and ARF1 decreased in neuronal tissues from postnatal day 10 (P10) to P28 (Figure S2).

Altogether, these results show that GBF1 is abundant in neuronal tissues and particularly in relevant MN pathology sites. Moreover, GBF1 levels during MN differentiation suggest that the protein plays an important yet unexplored role in neuronal development and maintenance.

All animal breeding and procedures were performed in accordance with the institutional animal care guidelines and the German animal welfare laws. They are approved under the reference numbers 84-02.04.2015.A378 and §4.18.002 of the State Agency for Nature, Environment, and Consumer Protection of the State North Rhine-Westphalia (LANUV NRW).

Given the important role of GBF1 in GA function and maintenance, and further considering that GBF1 depletion or inhibition has been linked with GA vesiculation and fragmentation,[32,52,53,56] we focused our functional analyses ascertaining the effect of GBF1 mutations on GA organization by using primary fibroblast cells established from skin biopsies. We were able to establish fibroblast cell lines from all the probands belonging to the four unrelated families reported in this study. Immunoblot analyses of GBF1 did not reveal significant differences between GBF1 mutant cell lines in comparison to WT control lines, except for the cell line heterozygous for p.Trp1175Ter, where a WT full-length and a potentially truncated smaller protein product can be observed (Figure S3). Notwithstanding this, immunostainings with the GBF1 antibody and the *cis* Golgi marker GM130 (Table S1) revealed the expected enrichment of GBF1 in the GA and a more diffuse cytoplasmic signal of the protein in all fibroblast lines. Moreover, all mutant fibroblast lines exhibited significantly increased proportions of cells with a marked dispersion of both GBF1 and GM130 signals (from 8% in control cells up to 28% to 46% in probands' fibroblasts), consistent with Golgi fragmentation (Figures 4A and 4B). Although the Golgi phenotype was slightly more pronounced in the fibroblast cell line derived from the proband with the p.Trp1175Ter alteration, possibly because of the truncating nature of the alteration, all probands' fibroblasts exhibited a marked GA phenotype and a general loss of the central Golgi ribbon stack. We postulate that Golgi fragmentation/vesiculation is the unifying pathogenic functional signature underlying *GBF1* heterozygous disease-associated variants.

In conclusion, our results support the association between *GBF1* pathogenic variants and the common phenotype of HMN and CMT2. *GBF1* not only expands the number of genetic loci associated with HMN/CMT2 but also corroborates Golgi fragmentation as a driver of length-dependent motor axonopathy.

Structural and functional alterations of the GA are currently recognized as an important pathological hallmark of various neurodegenerative diseases, including Parkinson, Alzheimer, Huntington, amyotrophic lateral sclerosis (ALS), spinal muscular atrophy (SMA), type-2 spinocerebellar ataxia (SCA2), SMALED2, and Creutzfeldt-Jakob diseases.[57,58] In general, GA defects are considered as early or preclinical indicators of neuronal loss and range from extensive Golgi unstacking, vesiculation, and ribbon disconnection to generalized Golgi atrophy (loss of Golgi membrane material). Loss of Golgi integrity can have a detrimental effect in cargo transport velocity,[59] mitosis completion,[54] autophagy regulation,[60] cell polarity, and migration.[61] Most precisely, in neurons, the GA is crucial for dendrite formation and growth, axonal polarity, and cell migration during brain development.[62–64]

Interestingly, *de novo* missense mutations affecting the GDP/GTP-binding site of ARF1 were found in three unrelated individuals and associated with periventricular

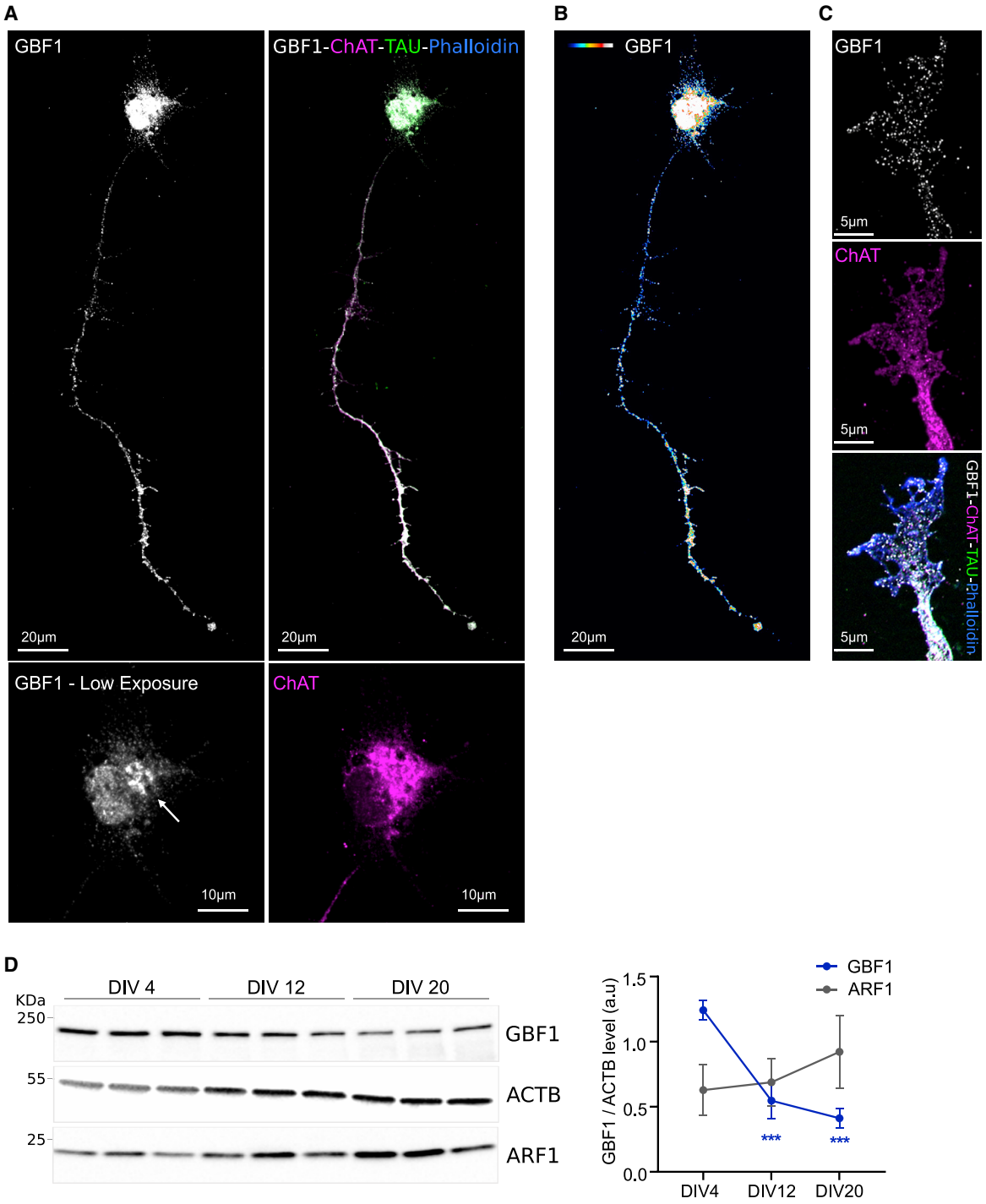


**Figure 3. Localization and GBF1 Abundance in Relevant Motor Neuropathology Tissues**

(A) GBF1 localization in primary MNs. Representative image of MNs isolated from WT E13.5 embryos cultured 7 days *in vitro* (DIV7). Immunostaining shows high abundance of GBF1 in the cell body, axon, and growth cone. Lower panels include a low-exposure image of GBF1 (marked with an arrow) that depicts protein enrichment in the GA and ChAT-positive immunoreactivity. Depicted stainings are GBF1 (white), ChAT (magenta), Tau (green), and phalloidin (blue). Scale bar represents 20 μm. Inset scale bar represents 10 μm.

(B) GBF1 fluorescent intensity is depicted with rainbow intensities to highlight MN zones of higher protein accumulation. Scale bar represents 20 μm

(C) GBF1 is abundantly present in the MN growth cone. Depicted stainings are GBF1 (white), ChAT (magenta), Tau (green), and Phalloidin (blue). Scale bar represents 20 μm.

(D) GBF1 expression decreases over time in differentiating primary MNs. MNs isolated from WT E13.5 embryos were cultured during 20 days in the presence of growth factors. Total protein lysates were collected at the indicated time points. Immunoblots were probed against GBF1 and ACTB as the normalization housekeeper. Graphs represent quantification of relative expression of GBF1. Bars show the mean ± SEM from three independent samples. Asterisk denotes statistical significance (***p = 0.001, two-tailed Student's t test) between the different time points compared to DIV4.

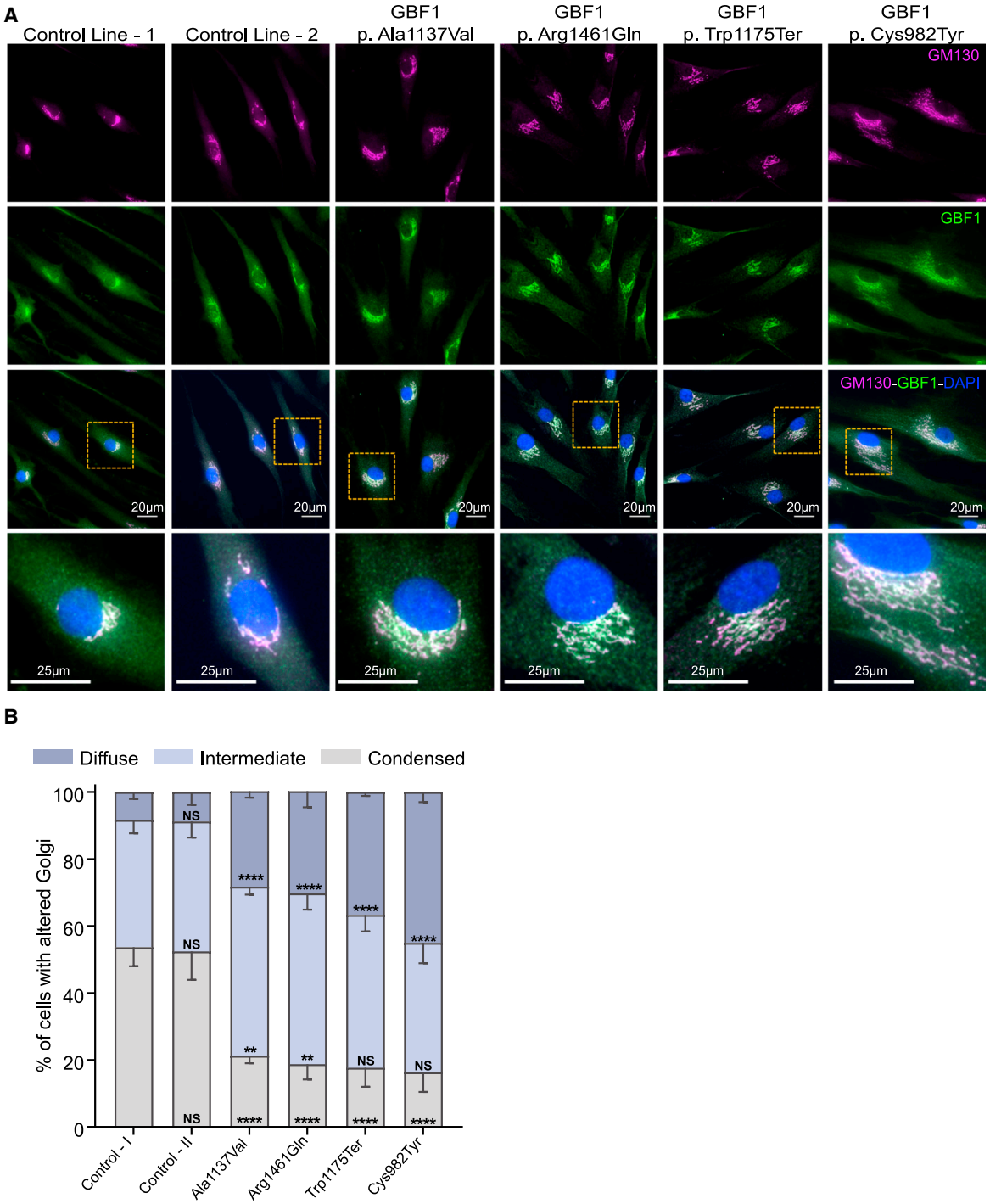


**Figure 4. Pathogenic GBF1 Variants Cause Golgi Fragmentation**

(A) Representative images of fibroblast cells derived from control or affected individuals. Immunostainings show GBF1 presence in the whole cell and enrichment in the GA region. Depicted stainings are GBF1 (green), GM130 (magenta), and nucleus (DAPI, blue). Scale bar represents 25 μm. Scale bar of magnification insets represents 25 μm. The dispersion of the GM130 signal was used to establish three categories of GA structure: condensed or no fragmentation, intermediate fragmentation, and diffuse or extensive fragmentation. Extensive fragmentation of the GA can be appreciated in magnified insets of representative images from affected fibroblast compared to control.

(B) GA structures were quantified in more than 300 cells representing at least three independent double-blinded experiments. Graph represents GA fragmentation quantification. Bars show mean ± SD. Asterisks denote statistical significance (**p = 0.01 and ****p = 0.0001, one-way ANOVA and Dunnett's correction for multiple comparisons). "NS" denotes no significance.

nodular heterotopia-8 (*PVNH8*, [MIM: 618185]), a neurologic disorder characterized by abnormal neuronal migration during brain development and concomitant delay in psychomotor development.[65] Similarly, bi-allelic variants in a second ARF1 activator, ADP-ribosylation factor guanine nucleotide exchange factor 2 (*ARFGEF2* [MIM: 605371]), were associated with proliferation and migration defects of cortical neurons, causing a severe malformation of the cerebral cortex known as periventricular heterotopia with microcephaly (ARPHM [MIM: 608097]).[66] Furthermore, individuals with severe SMALED2, as well as the *Bicd2*$^{-/-}$ mouse model, also exhibit profound cerebellar hypoplasia and cortical migration defects.[20,67–69] We postulate that *GBF1* pathogenic variants, similar to *ARF1*, *ARFGEF2*, and *BICD2* variants, could underlie migration defects in MNs, considering not only the abundance of the protein in the spinal cord but also the early developmental requirements thereof. As for BICD2-opathies, we previously described phenotypic extremes in individuals with the same *BICD2* pathogenic variants with very different levels of phenotypic severity, including a proband with an early onset severe phenotype and an asymptomatic parent.[20] Similarly, we observed phenotypic variability in our *GBF1* family pedigrees, although it remains unclear whether the asymptomatic mutation carriers in this study exhibit a discrete subclinical phenotype suggesting variable expression[70] or a complete absence of disease consistent with incomplete penetrance. Because of the late onset and mild course of the HMN/CMT2 phenotypes described here, a well-founded conclusion about the expressivity and penetrance of the disease could not be reached at this point. Another explanation regarding protective genetic modifiers abrogating the disease-onset or progression remains possible.

The molecular mechanism behind GBF1 mutations and Golgi fragmentation remains to be elucidated. Nevertheless, since GBF1 is a central player in molecular pathways that are necessary for GA maintenance, structure, and function, we hypothesize that pathogenic GBF1 mutations could drive GA pathology by compromising either the Golgi transport machinery or the microtubule control of Golgi structure and positioning. Indeed, traffic impairment between the Golgi, the endoplasmic reticulum (ER), and the ERGIC (ER-Golgi intermediate compartment), i.e., defects in COPI and COPII vesicle-coat complexes, can lead to severe GA structural defects.[71] In this respect, it is important to emphasize that the activation of ARF1 by GBF1 is crucial for the assembly of the COPI vesicle-coat complex at the Golgi and ERGIC membranes and that the inactivation or depletion of GBF1 causes COPI dissociation from membranes with concomitant GA fragmentation.[32,53,72]

On the other hand, the microtubule (MT) network is essential not only for the structural maintenance and positioning of the GA, but also for the anterograde and retrograde movement of cargo at the *cis* and *trans* Golgi networks.[73] In fact, MT depolymerization causes dispersion of the GA ribbon.[74] During neurodegeneration, fragmented Golgi structures appeared dispersed throughout the cell, further implying a disconnection of the GA and the cytoskeleton.[58] Most interestingly, the GA, other than the centrosome, is a center for MT nucleation and is of particular relevance for polarized cells, such as the MN.[75] Indeed, Golgi outposts of a centrosomal MT polymerization shape dendrite morphology and could explain the susceptibility of MNs and other neuronal populations to Golgi defects. Another possibility that cannot be ruled out is that Golgi fragmentation is a secondary phenotype derived from the impairment of another cellular process or organelle. Mitochondrial defects have been proposed as a trigger of GA fragmentation and the activation of the Golgi stress response,[76,77] and GBF1 inhibition impairs dynein and MIRO (1 and 2)-dependent retrograde mitochondrial transport along MTs towards the microtubule organizing center.[36] Moreover, mitochondrial defects in Mitofusin 2 (*MFN2* [MIM: 608507]) and ganglioside-induced differentiation-associated-protein 1 (*GDAP1* [MIM: 606598]) are associated with CMT2.[78,79]

GBF1 interactions with proteins of the secretory pathways, molecular motors, and mitochondrial regulators hold the key to understanding the molecular determinants of Golgi fragmentation and represent promising HMN-causative gene candidates that remain to be discovered.

## Data and Code Availability

The variants were deposited in Clinvar and are accessible via the accession codes VCV000972907, VCV000973612, VCV000972904, and VCV000975152. NGS dataset of family 1 is available in the European Genome-phenome Archive (EGA) under following accession codes: EGAN00001366899, EGAN00001366900, EGAN0000 1366901. Sequence datasets of other families might be available from the corresponding author upon request. Please contact M.K. and B.W. for further information.

### Supplemental Data

Supplemental Data can be found online at https://doi.org/10.1016/j.ajhg.2020.08.018.


### Acknowledgments

We would like to thank the family members described herein for participating in this study. We thank all our clinical collaborators for the support at clinical follow-up, diagnostics, and the genetic analysis. We furthermore thank the Regional Computing Center of the University of Cologne (RZZK) for providing computing time and storage on the CHEOPS high performance computing cluster. This work was supported by the Deutsche Forschungsgemeinschaft (Wi945/19-1 and RTG 1960 to B.W.), NRW Innovation Award (B.W.), the European Community's Seventh Framework Programme (FP7/2007–2013) under grant 2012-305121 (NEUROMICS) (B.W. and J.B.), the Center for Molecular Medicine Cologne (C18 to B.W. and M.K.), the Association Belge contre les Maladies

Neuromusculaire (ABMM)—Aide à la Recherche ASBL (2017-2018/05) (D.B. and J.B.). J.B. is supported by a Senior Clinical Researcher mandate of the Research Fund-Flanders (FWO) under grant 1805016N. We are thankful for access to the GENESIS analysis platform and Varbank analysis platform.

## Declaration of Interests

C.G.-J. is a full-time employee of the Regeneron Genetics Center and receives stock options as part of compensation. All other authors declare no competing interests

Received: May 29, 2020
Accepted: August 19, 2020
Published: September 15, 2020

## Web Resources

Combined Annotation Dependent Depletion (CADD), https://cadd.gs.washington.edu
Ensembl Genome Browser, http://www.ensembl.org/index.html
European Genome-Phenome Archive, https://ega-archive.org/
Inherited Neuropathy Variant Browser, http://hihg.med.miami.edu/code/http/cmt/public_html/index.html
Multiple sequence alignment CLUSTALW2, https://www.ebi.ac.uk/Tools/msa/clustalw2/
Muscle Gene Table, http://musclegenetable.fr
Neuromics Consortium, https://rd-neuromics.eu/
Online Mendelian Inheritance in an (OMIM), https://www.omim.org/
RD Connect Database, https://platform.rd-connect.eu/
The Genome Aggregation Database, https://gnomad.broadinstitute.org/
Varbank Variant Analysis Platform, https://varbank.ccg.uni-koeln.de/varbank2/

## References

1. Landrieu, P., Baets, J., and De Jonghe, P. (2013). Hereditary motor-sensory, motor, and sensory neuropathies in childhood. Handb. Clin. Neurol. *113*, 1413–1432.
2. Klein, C.J., Duan, X., and Shy, M.E. (2013). Inherited neuropathies: clinical overview and update. Muscle Nerve *48*, 604–622.
3. Harding, A.E., and Thomas, P.K. (1980). Genetic aspects of hereditary motor and sensory neuropathy (types I and II). J. Med. Genet. *17*, 329–336.
4. Harding, A.E. (2005). Inherited Neuronal Atrophy and Degeneration Predominantly of Lower Motor Neurons* A2 - Dyck, Peter J. In Peripheral Neuropathy, Fourth Edition, P.K. Thomas, ed. *(Philadelphia: W.B. Saunders), pp. 1603–1621*.
5. Bansagi, B., Griffin, H., Whittaker, R.G., Antoniadi, T., Evangelista, T., Miller, J., Greenslade, M., Forester, N., Duff, J., Bradshaw, A., et al. (2017). Genetic heterogeneity of motor neuropathies. Neurology *88*, 1226–1234.
6. Gonzaga-Jauregui, C., Harel, T., Gambin, T., Kousi, M., Griffin, L.B., Francescatto, L., Ozes, B., Karaca, E., Jhangiani, S.N., Bainbridge, M.N., et al.; Baylor-Hopkins Center for Mendelian Genomics (2015). Exome Sequence Analysis Suggests that Genetic Burden Contributes to Phenotypic Variability and Complex Neuropathy. Cell Rep. *12*, 1169–1183.
7. Irobi, J., Van Impe, K., Seeman, P., Jordanova, A., Dierick, I., Verpoorten, N., Michalik, A., De Vriendt, E., Jacobs, A., Van Gerwen, V., et al. (2004). Hot-spot residue in small heat-shock protein 22 causes distal motor neuropathy. Nat. Genet. *36*, 597–601.
8. Evgrafov, O.V., Mersiyanova, I., Irobi, J., Van Den Bosch, L., Dierick, I., Leung, C.L., Schagina, O., Verpoorten, N., Van Impe, K., Fedotov, V., et al. (2004). Mutant small heat-shock protein 27 causes axonal Charcot-Marie-Tooth disease and distal hereditary motor neuropathy. Nat. Genet. *36*, 602–606.
9. Ackerley, S., James, P.A., Kalli, A., French, S., Davies, K.E., and Talbot, K. (2006). A mutation in the small heat-shock protein HSPB1 leading to distal hereditary motor neuronopathy disrupts neurofilament assembly and the axonal transport of specific cellular cargoes. Hum. Mol. Genet. *15*, 347–354.
10. Irobi, J., Almeida-Souza, L., Asselbergh, B., De Winter, V., Goethals, S., Dierick, I., Krishnan, J., Timmermans, J.P., Robberecht, W., De Jonghe, P., et al. (2010). Mutant HSPB8 causes motor neuron-specific neurite degeneration. Hum. Mol. Genet. *19*, 3254–3265.
11. Puls, I., Jonnakuty, C., LaMonte, B.H., Holzbaur, E.L., Tokito, M., Mann, E., Floeter, M.K., Bidus, K., Drayna, D., Oh, S.J., et al. (2003). Mutant dynactin in motor neuron disease. Nat. Genet. *33*, 455–456.
12. Levy, J.R., Sumner, C.J., Caviston, J.P., Tokito, M.K., Ranganathan, S., Ligon, L.A., Wallace, K.E., LaMonte, B.H., Harmison, G.G., Puls, I., et al. (2006). A motor neuron disease-associated mutation in p150Glued perturbs dynactin function and induces protein aggregation. J. Cell Biol. *172*, 733–745.
13. Calvo, J., Funalot, B., Ouvrier, R.A., Lazaro, L., Toutain, A., De Mas, P., Bouche, P., Gilbert-Dussardier, B., Arne-Bes, M.C., Carrière, J.P., et al. (2009). Genotype-phenotype correlations in Charcot-Marie-Tooth disease type 2 caused by mitofusin 2 mutations. Arch. Neurol. *66*, 1511–1516.
14. Claeys, K.G., Züchner, S., Kennerson, M., Berciano, J., Garcia, A., Verhoeven, K., Storey, E., Merory, J.R., Bienfait, H.M., Lammens, M., et al. (2009). Phenotypic spectrum of dynamin 2 mutations in Charcot-Marie-Tooth neuropathy. Brain *132*, 1741–1752.
15. Charlesworth, G., Balint, B., Mencacci, N.E., Carr, L., Wood, N.W., and Bhatia, K.P. (2016). SLC25A46 mutations underlie progressive myoclonic ataxia with optic atrophy and neuropathy. Mov. Disord. *31*, 1249–1251.
16. Martinez-Carrera, L.A., and Wirth, B. (2015). Dominant spinal muscular atrophy is caused by mutations in BICD2, an important golgin protein. Front. Neurosci. *9*, 401.
17. Neveling, K., Martinez-Carrera, L.A., Hölker, I., Heister, A., Verrips, A., Hosseini-Barkooie, S.M., Gilissen, C., Vermeer, S., Pennings, M., Meijer, R., et al. (2013). Mutations in BICD2, which encodes a golgin and important motor adaptor, cause congenital autosomal-dominant spinal muscular atrophy. Am. J. Hum. Genet. *92*, 946–954.
18. Peeters, K., Litvinenko, I., Asselbergh, B., Almeida-Souza, L., Chamova, T., Geuens, T., Ydens, E., Zimoń, M., Irobi, J., De Vriendt, E., et al. (2013). Molecular defects in the motor adaptor BICD2 cause proximal spinal muscular atrophy with autosomal-dominant inheritance. Am. J. Hum. Genet. *92*, 955–964.
19. Oates, E.C., Rossor, A.M., Hafezparast, M., Gonzalez, M., Speziani, F., MacArthur, D.G., Lek, M., Cottenie, E., Scoto, M., Foley, A.R., et al.; UK10K (2013). Mutations in BICD2 cause

dominant congenital spinal muscular atrophy and hereditary spastic paraplegia. Am. J. Hum. Genet. *92*, 965–973.
20. Storbeck, M., Horsberg Eriksen, B., Unger, A., Hölker, I., Aukrust, I., Martínez-Carrera, L.A., Linke, W.A., Ferbert, A., Heller, R., Vorgerd, M., et al. (2017). Phenotypic extremes of BICD2-opathies: from lethal, congenital muscular atrophy with arthrogryposis to asymptomatic with subclinical features. Eur. J. Hum. Genet. *25*, 1040–1048.
21. Martinez Carrera, L.A., Gabriel, E., Donohoe, C.D., Hölker, I., Mariappan, A., Storbeck, M., Uhlirova, M., Gopalakrishnan, J., and Wirth, B. (2018). Novel insights into SMALED2: BICD2 mutations increase microtubule stability and cause defects in axonal and NMJ development. Hum. Mol. Genet. *27*, 1772–1784.
22. Hoogenraad, C.C., and Akhmanova, A. (2016). Bicaudal D Family of Motor Adaptors: Linking Dynein Motility to Cargo Binding. Trends Cell Biol. *26*, 327–340.
23. Karakaya, M., Storbeck, M., Strathmann, E.A., Delle Vedove, A., Hölker, I., Altmueller, J., Naghiyeva, L., Schmitz-Steinkrüger, L., Vezyroglou, K., Motameny, S., et al. (2018). Targeted sequencing with expanded gene profile enables high diagnostic yield in non-5q-spinal muscular atrophies. Hum. Mutat. *39*, 1284–1298.
24. Gonzalez, M., Falk, M.J., Gai, X., Postrel, R., Schüle, R., and Zuchner, S. (2015). Innovative genomic collaboration using the GENESIS (GEM.app) platform. Hum. Mutat. *36*, 950–956.
25. Strauss, K.A., Gonzaga-Jauregui, C., Brigatti, K.W., Williams, K.B., King, A.K., Van Hout, C., Robinson, D.L., Young, M., Praveen, K., Heaps, A.D., et al. (2018). Genomic diagnostics within a medically underserved population: efficacy and implications. Genet. Med. *20*, 31–41.
26. Sobreira, N., Schiettecatte, F., Valle, D., and Hamosh, A. (2015). GeneMatcher: a matching tool for connecting investigators with an interest in the same gene. Hum. Mutat. *36*, 928–930.
27. Donaldson, J.G., and Jackson, C.L. (2011). ARF family G proteins and their regulators: roles in membrane transport, development and disease. Nat. Rev. Mol. Cell Biol. *12*, 362–375.
28. Donaldson, J.G., and Klausner, R.D. (1994). ARF: a key regulatory switch in membrane traffic and organelle structure. Curr. Opin. Cell Biol. *6*, 527–532.
29. García-Mata, R., Szul, T., Alvarez, C., and Sztul, E. (2003). ADP-ribosylation factor/COPI-dependent events at the endoplasmic reticulum-Golgi interface are regulated by the guanine nucleotide exchange factor GBF1. Mol. Biol. Cell *14*, 2250–2261.
30. Szul, T., Grabski, R., Lyons, S., Morohashi, Y., Shestopal, S., Lowe, M., and Sztul, E. (2007). Dissecting the role of the ARF guanine nucleotide exchange factor GBF1 in Golgi biogenesis and protein trafficking. J. Cell Sci. *120*, 3929–3940.
31. Kawamoto, K., Yoshida, Y., Tamaki, H., Torii, S., Shinotsuka, C., Yamashina, S., and Nakayama, K. (2002). GBF1, a guanine nucleotide exchange factor for ADP-ribosylation factors, is localized to the cis-Golgi and involved in membrane association of the COPI coat. Traffic *3*, 483–495.
32. Manolea, F., Claude, A., Chun, J., Rosas, J., and Melançon, P. (2008). Distinct functions for Arf guanine nucleotide exchange factors at the Golgi complex: GBF1 and BIGs are required for assembly and maintenance of the Golgi stack and trans-Golgi network, respectively. Mol. Biol. Cell *19*, 523–535.
33. Yadav, S., Puthenveedu, M.A., and Linstedt, A.D. (2012). Golgin160 recruits the dynein motor to position the Golgi apparatus. Dev. Cell *23*, 153–165.
34. Bouvet, S., Golinelli-Cohen, M.P., Contremoulins, V., and Jackson, C.L. (2013). Targeting of the Arf-GEF GBF1 to lipid droplets and Golgi membranes. J. Cell Sci. *126*, 4794–4805.
35. Ackema, K.B., Hench, J., Böckler, S., Wang, S.C., Sauder, U., Mergentaler, H., Westermann, B., Bard, F., Frank, S., and Spang, A. (2014). The small GTPase Arf1 modulates mitochondrial morphology and function. EMBO J. *33*, 2659–2675.
36. Walch, L., Pellier, E., Leng, W., Lakisic, G., Gautreau, A., Contremoulins, V., Verbavatz, J.M., and Jackson, C.L. (2018). GBF1 and Arf1 interact with Miro and regulate mitochondrial positioning within cells. Sci. Rep. *8*, 17121.
37. Gupta, G.D., Swetha, M.G., Kumari, S., Lakshminarayan, R., Dey, G., and Mayor, S. (2009). Analysis of endocytic pathways in Drosophila cells reveals a conserved role for GBF1 in internalization via GEECs. PLoS ONE *4*, e6768.
38. Witkos, T.M., Chan, W.L., Joensuu, M., Rhiel, M., Pallister, E., Thomas-Oates, J., Mould, A.P., Mironov, A.A., Biot, C., Guerardel, Y., et al. (2019). GORAB scaffolds COPI at the trans-Golgi for efficient enzyme recycling and correct protein glycosylation. Nat. Commun. *10*, 127.
39. Ferlin, J., Farhat, R., Belouzard, S., Cocquerel, L., Bertin, A., Hober, D., Dubuisson, J., and Rouillé, Y. (2018). Investigation of the role of GBF1 in the replication of positive-sense single-stranded RNA viruses. J. Gen. Virol. *99*, 1086–1096.
40. Belov, G.A., Kovtunovych, G., Jackson, C.L., and Ehrenfeld, E. (2010). Poliovirus replication requires the N-terminus but not the catalytic Sec7 domain of ArfGEF GBF1. Cell. Microbiol. *12*, 1463–1479.
41. Goueslain, L., Alsaleh, K., Horellou, P., Roingeard, P., Descamps, V., Duverlie, G., Ciczora, Y., Wychowski, C., Dubuisson, J., and Rouillé, Y. (2010). Identification of GBF1 as a cellular factor required for hepatitis C virus RNA replication. J. Virol. *84*, 773–787.
42. Iglesias, N.G., Mondotte, J.A., Byk, L.A., De Maio, F.A., Samsa, M.M., Alvarez, C., and Gamarnik, A.V. (2015). Dengue Virus Uses a Non-Canonical Function of the Host GBF1-Arf-COPI System for Capsid Protein Accumulation on Lipid Droplets. Traffic *16*, 962–977.
43. de Wilde, A.H., Wannee, K.F., Scholte, F.E., Goeman, J.J., Ten Dijke, P., Snijder, E.J., Kikkert, M., and van Hemert, M.J. (2015). A Kinome-Wide Small Interfering RNA Screen Identifies Proviral and Antiviral Host Factors in Severe Acute Respiratory Syndrome Coronavirus Replication, Including Double-Stranded RNA-Activated Protein Kinase and Early Secretory Pathway Proteins. J. Virol. *89*, 8318–8333.
44. Ramaen, O., Joubert, A., Simister, P., Belgareh-Touzé, N., Olivares-Sanchez, M.C., Zeeh, J.C., Chantalat, S., Golinelli-Cohen, M.P., Jackson, C.L., Biou, V., and Cherfils, J. (2007). Interactions between conserved domains within homodimers in the BIG1, BIG2, and GBF1 Arf guanine nucleotide exchange factors. J. Biol. Chem. *282*, 28834–28842.
45. Bhatt, J.M., Viktorova, E.G., Busby, T., Wyrozumska, P., Newman, L.E., Lin, H., Lee, E., Wright, J., Belov, G.A., Kahn, R.A., and Sztul, E. (2016). Oligomerization of the Sec7 domain Arf guanine nucleotide exchange factor GBF1 is dispensable for Golgi localization and function but regulates degradation. Am. J. Physiol. Cell Physiol. *310*, C456–C469.
46. Szul, T., Garcia-Mata, R., Brandon, E., Shestopal, S., Alvarez, C., and Sztul, E. (2005). Dissection of membrane dynamics

of the ARF-guanine nucleotide exchange factor GBF1. Traffic *6*, 374–385.
47. Holloway, Z.G., Grabski, R., Szul, T., Styers, M.L., Coventry, J.A., Monaco, A.P., and Sztul, E. (2007). Activation of ADP-ribosylation factor regulates biogenesis of the ATP7A-containing trans-Golgi network compartment and its Cu-induced trafficking. Am. J. Physiol. Cell Physiol. *293*, C1753–C1767.
48. Zhao, X., Claude, A., Chun, J., Shields, D.J., Presley, J.F., and Melançon, P. (2006). GBF1, a cis-Golgi and VTCs-localized ARF-GEF, is implicated in ER-to-Golgi protein traffic. J. Cell Sci. *119*, 3743–3753.
49. Quilty, D., Chan, C.J., Yurkiw, K., Bain, A., Babolmorad, G., and Melançon, P. (2018). The Arf-GDP-regulated recruitment of GBF1 to Golgi membranes requires domains HDS1 and HDS2 and a Golgi-localized protein receptor. J. Cell Sci. *132*, jcs208199.
50. Meissner, J.M., Bhatt, J.M., Lee, E., Styers, M.L., Ivanova, A.A., Kahn, R.A., and Sztul, E. (2018). The ARF guanine nucleotide exchange factor GBF1 is targeted to Golgi membranes through a PIP-binding domain. J. Cell Sci. *131*, jcs210245.
51. Pocognoni, C.A., Viktorova, E.G., Wright, J., Meissner, J.M., Sager, G., Lee, E., Belov, G.A., and Sztul, E. (2018). Highly conserved motifs within the large Sec7 ARF guanine nucleotide exchange factor GBF1 target it to the Golgi and are critical for GBF1 activity. Am. J. Physiol. Cell Physiol. *314*, C675–C689.
52. Citterio, C., Vichi, A., Pacheco-Rodriguez, G., Aponte, A.M., Moss, J., and Vaughan, M. (2008). Unfolded protein response and cell death after depletion of brefeldin A-inhibited guanine nucleotide-exchange protein GBF1. Proc. Natl. Acad. Sci. USA *105*, 2877–2882.
53. Chen, J., Wu, X., Yao, L., Yan, L., Zhang, L., Qiu, J., Liu, X., Jia, S., and Meng, A. (2017). Impairment of Cargo Transportation Caused by *gbf1* Mutation Disrupts Vascular Integrity and Causes Hemorrhage in Zebrafish Embryos. J. Biol. Chem. *292*, 2315–2327.
54. Magliozzi, R., Carrero, Z.I., Low, T.Y., Yuniati, L., Valdes-Quezada, C., Kruiswijk, F., van Wijk, K., Heck, A.J.R., Jackson, C.L., and Guardavaccaro, D. (2018). Inheritance of the Golgi Apparatus and Cytokinesis Are Controlled by Degradation of GBF1. Cell Rep. *23*, 3381–3391.e4.
55. Mansour, S.J., Herbrick, J.A., Scherer, S.W., and Melançon, P. (1998). Human GBF1 is a ubiquitously expressed gene of the sec7 domain family mapping to 10q24. Genomics *54*, 323–327.
56. Ackema, K.B., Sauder, U., Solinger, J.A., and Spang, A. (2013). The ArfGEF GBF-1 Is Required for ER Structure, Secretion and Endocytic Transport in C. elegans. PLoS ONE *8*, e67076.
57. Rabouille, C., and Haase, G. (2016). Editorial: Golgi Pathology in Neurodegenerative Diseases. Front. Neurosci. *9*, 489.
58. Martínez-Menárguez, J.A., Tomás, M., Martínez-Martínez, N., and Martínez-Alonso, E. (2019). Golgi Fragmentation in Neurodegenerative Diseases: Is There a Common Cause? Cells *8*, 748.
59. Lavieu, G., Dunlop, M.H., Lerich, A., Zheng, H., Bottanelli, F., and Rothman, J.E. (2014). The Golgi ribbon structure facilitates anterograde transport of large cargoes. Mol. Biol. Cell *25*, 3028–3036.
60. Gosavi, P., Houghton, F.J., McMillan, P.J., Hanssen, E., and Gleeson, P.A. (2018). The Golgi ribbon in mammalian cells negatively regulates autophagy by modulating mTOR activity. J. Cell Sci. *131*, jcs211987.
61. Saraste, J., and Prydz, K. (2019). A New Look at the Functional Organization of the Golgi Ribbon. Front. Cell Dev. Biol. *7*, 171.
62. Horton, A.C., Rácz, B., Monson, E.E., Lin, A.L., Weinberg, R.J., and Ehlers, M.D. (2005). Polarized secretory trafficking directs cargo for asymmetric dendrite growth and morphogenesis. Neuron *48*, 757–771.
63. Rao, S., Kirschen, G.W., Szczurkowska, J., Di Antonio, A., Wang, J., Ge, S., and Shelly, M. (2018). Repositioning of Somatic Golgi Apparatus Is Essential for the Dendritic Establishment of Adult-Born Hippocampal Neurons. J. Neurosci. *38*, 631–647.
64. Ye, B., Zhang, Y., Song, W., Younger, S.H., Jan, L.Y., and Jan, Y.N. (2007). Growing dendrites and axons differ in their reliance on the secretory pathway. Cell *130*, 717–729.
65. Ge, X., Gong, H., Dumas, K., Litwin, J., Phillips, J.J., Waisfisz, Q., Weiss, M.M., Hendriks, Y., Stuurman, K.E., Nelson, S.F., et al. (2016). Missense-depleted regions in population exomes implicate ras superfamily nucleotide-binding protein alteration in patients with brain malformation. NPJ Genom. Med. *1*, 16036.
66. Banne, E., Atawneh, O., Henneke, M., Brockmann, K., Gärtner, J., Elpeleg, O., and Edvardson, S. (2013). West syndrome, microcephaly, grey matter heterotopia and hypoplasia of corpus callosum due to a novel ARFGEF2 mutation. J. Med. Genet. *50*, 772–775.
67. Ravenscroft, G., Di Donato, N., Hahn, G., Davis, M.R., Craven, P.D., Poke, G., Neas, K.R., Neuhann, T.M., Dobyns, W.B., and Laing, N.G. (2016). Recurrent de novo BICD2 mutation associated with arthrogryposis multiplex congenita and bilateral perisylvian polymicrogyria. Neuromuscul. Disord. *26*, 744–748.
68. Fiorillo, C., Moro, F., Brisca, G., Accogli, A., Trucco, F., Trovato, R., Pedemonte, M., Severino, M., Catala, M., Capra, V., et al. (2016). Beyond spinal muscular atrophy with lower extremity dominance: cerebellar hypoplasia associated with a novel mutation in BICD2. Eur. J. Neurol. *23*, e19–e21.
69. Rossor, A.M., Sleigh, J.N., Groves, M., Muntoni, F., Reilly, M.M., Hoogenraad, C.C., and Schiavo, G. (2020). Loss of BICD2 in muscle drives motor neuron loss in a developmental form of spinal muscular atrophy. Acta Neuropathol. Commun. *8*, 34.
70. Lupski, J.R., Reid, J.G., Gonzaga-Jauregui, C., Rio Deiros, D., Chen, D.C., Nazareth, L., Bainbridge, M., Dinh, H., Jing, C., Wheeler, D.A., et al. (2010). Whole-genome sequencing in a patient with Charcot-Marie-Tooth neuropathy. N. Engl. J. Med. *362*, 1181–1191.
71. Ward, T.H., Polishchuk, R.S., Caplan, S., Hirschberg, K., and Lippincott-Schwartz, J. (2001). Maintenance of Golgi structure and function depends on the integrity of ER export. J. Cell Biol. *155*, 557–570.
72. Kaczmarek, B., Verbavatz, J.M., and Jackson, C.L. (2017). GBF1 and Arf1 function in vesicular trafficking, lipid homoeostasis and organelle dynamics. Biol. Cell *109*, 391–399.
73. Fourriere, L., Jimenez, A.J., Perez, F., and Boncompain, G. (2020). The role of microtubules in secretory protein transport. J. Cell Sci. *133*, jcs237016.
74. Cole, N.B., Sciaky, N., Marotta, A., Song, J., and Lippincott-Schwartz, J. (1996). Golgi dispersal during microtubule disruption: regeneration of Golgi stacks at peripheral endoplasmic reticulum exit sites. Mol. Biol. Cell *7*, 631–650.
75. Ori-McKenney, K.M., Jan, L.Y., and Jan, Y.N. (2012). Golgi outposts shape dendrite morphology by functioning as sites of acentrosomal microtubule nucleation in neurons. Neuron *76*, 921–930.

76. Machamer, C.E. (2015). The Golgi complex in stress and death. Front. Neurosci. *9*, 421.
77. Nakagomi, S., Barsoum, M.J., Bossy-Wetzel, E., Sütterlin, C., Malhotra, V., and Lipton, S.A. (2008). A Golgi fragmentation pathway in neurodegeneration. Neurobiol. Dis. *29*, 221–231.
78. Cassereau, J., Chevrollier, A., Gueguen, N., Desquiret, V., Verny, C., Nicolas, G., Dubas, F., Amati-Bonneau, P., Reynier, P., Bonneau, D., and Procaccio, V. (2011). Mitochondrial dysfunction and pathophysiology of Charcot-Marie-Tooth disease involving GDAP1 mutations. Exp. Neurol. *227*, 31–41.
79. Stuppia, G., Rizzo, F., Riboldi, G., Del Bo, R., Nizzardo, M., Simone, C., Comi, G.P., Bresolin, N., and Corti, S. (2015). MFN2-related neuropathies: Clinical features, molecular pathogenesis and therapeutic perspectives. J. Neurol. Sci. *356*, 7–18.

**The American Journal of Human Genetics, Volume *107***

## Supplemental Data

# *De Novo* and Inherited Variants in *GBF1* are Associated with Axonal Neuropathy Caused by Golgi Fragmentation

**Natalia Mendoza-Ferreira, Mert Karakaya, Nur Cengiz, Danique Beijer, Karlla W. Brigatti, Claudia Gonzaga-Jauregui, Nico Fuhrmann, Irmgard Hölker, Maximilian P. Thelen, Sebastian Zetzsche, Roman Rombo, Erik G. Puffenberger, Peter De Jonghe, Tine Deconinck, Stephan Zuchner, Kevin A. Strauss, Vincent Carson, Bertold Schrank, Gilbert Wunderlich, Jonathan Baets, and Brunhilde Wirth**

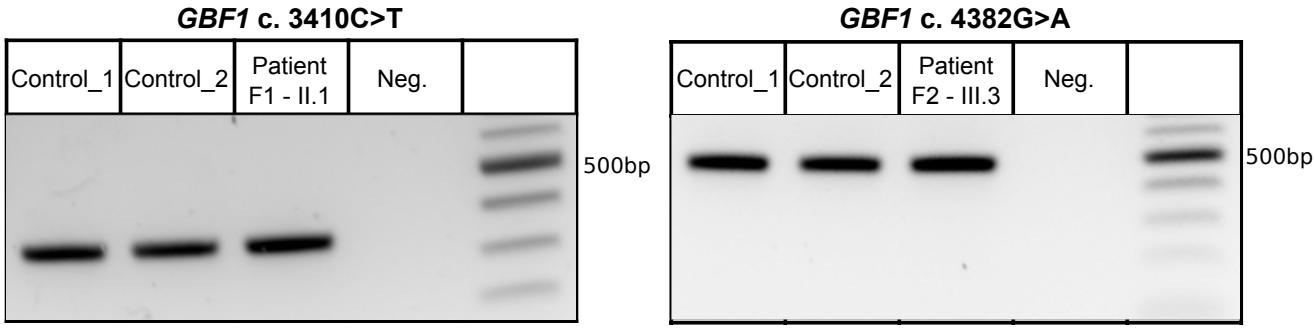


**Figure S1. *GBF1* variants c.3410C>T and c.4382G>A do not affect splicing.**

Determination of *GBF1* c.3410C>T and *GBF1* c.4382G>A transcripts by semi-quantitative RT-PCR. RNA was isolated from cultured fibroblast cell lines from *GBF1* index probands and control individuals. No additional PCR amplification products, indicating potential miss-splicing events, were observed.

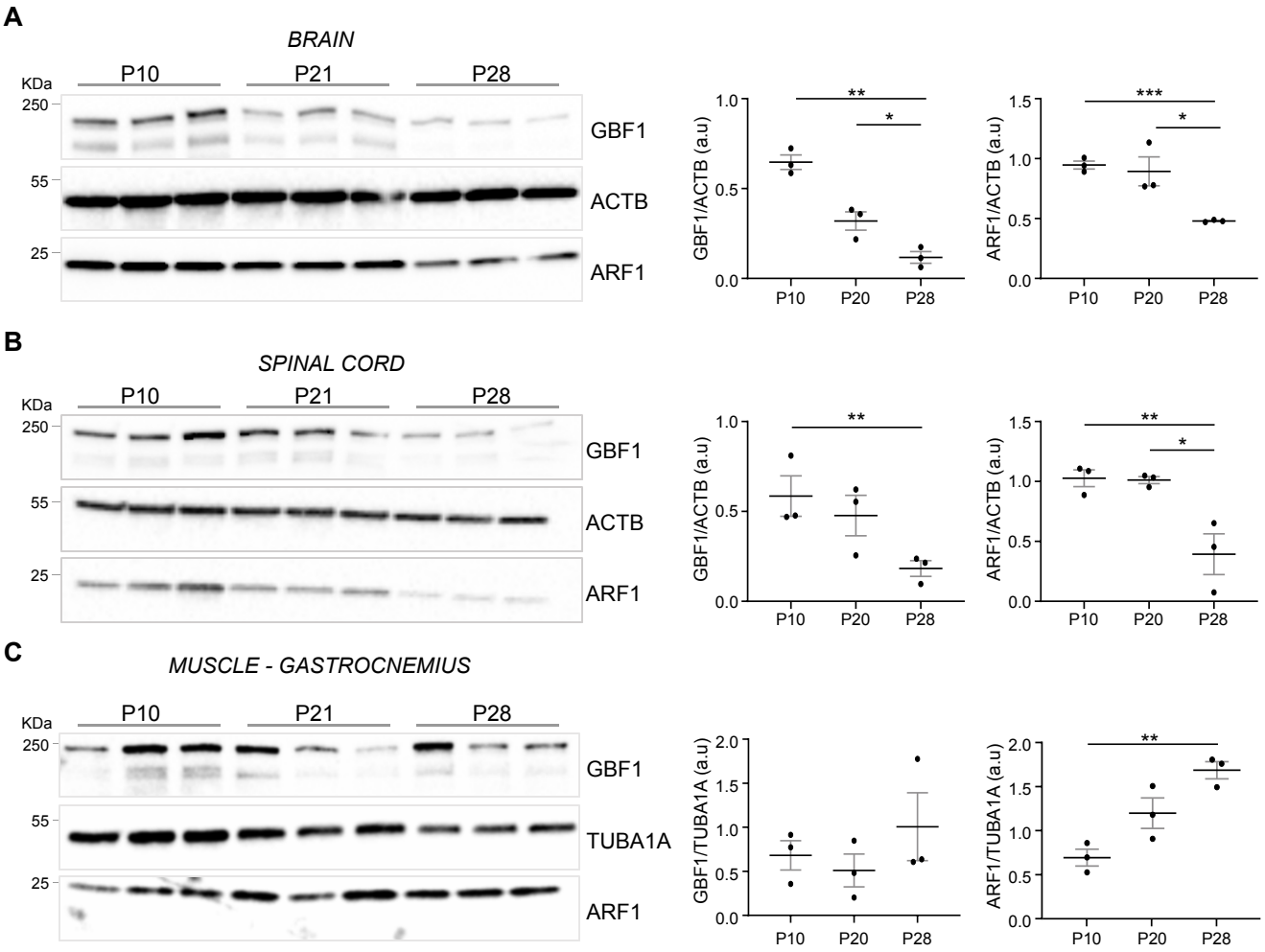


**Figure S2. GBF1 levels in mouse brain, spinal cord and muscle.**

Western blot analysis of brain **(A)**, spinal cord **(B)** and gastrocnemius muscle **(C)** from P10, P21, and P28 wild type mice. GBF1 and ARF1 levels were quantified by the ratio to the housekeepers ACTB or TUBA1A (for muscle). Blots quantifications of relative protein abundance are given in the graphs on the right. Bars show the mean ± SD from three independent samples. "*" denotes statistical significance ($^{*}$ $p \leq 0.05$, $^{**}$ $p = 0.01$, and $^{***}$ $p = 0.001$ unpaired two-tailed Student t test) between the different time points compared to P10. P= post-natal.

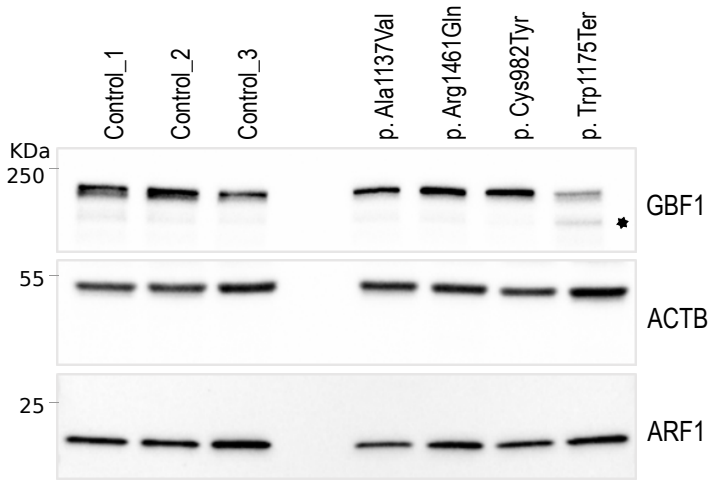


**Figure S3. GBF1 levels in probands-derived fibroblasts.**

Western blot analysis of total protein lysates isolated from fibroblast cell lines of three controls and the four probands. Blots were stained with antibodies against GBF1, ARF1, and the housekeeping protein ACTB to assure equal loading. * = potentially truncated version of GBF1

| Application | Antibody / Dye | Dilution | Manufacturer | Catalogue number |
|---|---|---|---|---|
| Western blot | mouse α-GBF1 (25) | 1:1000 o/n 4°C | Santa Cruz Biotechnology | sc-136240 |
| | mouse α-ARF1 (ARFS 1A9/5) | 1:500 o/n 4°C | Santa Cruz Biotechnology | sc-53168 |
| | mouse α-Golgin 160 (C-8) | 1:500 o/n 4°C | Santa Cruz Biotechnology | sc-374596 |
| | mouse α-β-actin HRP conjugated | 1:5000 1h / RT | Proteintech | HRP-60008 |
| | mouse α-TUBA1A | 1:1000 1h / RT | Sigma Aldrich | T9026 |
| Cells / MNs Immunostaining | rabbit α-GBF1 | 1:100 o/n 4°C | Abcam | ab 86071 |
| | mouse α-GM130 | 1:100 o/n 4°C | BD Transduction Laboratories | cat 610822 |
| General Secondary antibodies / dyes | α-mouse-HRP | 1:2500 1h / RT | Dianova | 115-035-146 |
| | α-rabbit-HRP | 1:2500 1h / RT | Cell signaling | 7074P2 |
| | Phalloidin AlexaFluor 647 | 1:70 1h / RT | Thermo Fisher Scientific | A22287 |
| | rabbit α-AlexaFluor-488 | 1:500 1h / RT | Thermo Fisher Scientific | A21206 |
| | mouse α-AlexaFluor-488 | 1:500 1h / RT | Thermo Fisher Scientific | A10680 |
| | mouse α-AlexaFluor-568 | 1:500 1h / RT | Thermo Fisher Scientific | A11031 |
| | rabbit α-AlexaFluor-568 | 1:500 1h / RT | Thermo Fisher Scientific | A10042 |
| | mouse α-AlexaFluor-647 | 1:500 1h / RT | Thermo Fisher Scientific | A31571 |

**Table S1. Antibodies and dyes used in this study**

## Supplemental Materials and Methods

### Ethics approval and informed consent

The study protocol for family 1 and 4 were approved by the University of Cologne Ethics Committee (Reference number: 13-022) and written informed consent for genetic analysis and clinical images from each studied subject were obtained.

Family 2 consented to genetic diagnostic follow-up by Antwerp University Hospital (UZA) and University of Antwerp (UA) and studies were approved under UZA/UA ethical committee 15/37/375.

Family 3 were consented to whole exome sequencing at Regeneron by the research team at the Clinic for Special Children under protocol 2008-095-CSC, which has IRB oversight through Lancaster General Hospital in Lancaster, Pennsylvania, USA.

All animal breedings and procedures were performed in accordance with the institutional animal care guidelines and the German animal welfare laws. They are approved under the reference numbers 84-02.04.2015.A378 and UniKoeln_Anzeige §4.18.002 of the LANUV (Landesamt für Natur, Umwelt und Verbraucherschutz NRW) state agency of North-Rhine-Westphalia.

### Genetic analyses

Whole genome sequencing (WGS) was performed as previously described in.[1] Samples were prepared for WGS using Illumina´s TruSeq PCR-Free sample preparation kit (https://www.illumina.com/products/by-type/sequencing-kits/library-prep-kits/truseq-dna-pcr-free.html). 1 µg of gDNA was fragmented to a mean target size of 350-450 bp using a Covaris E220 instrument, followed by end-repair, 3'-adenylation and ligation of indexed sequencing adaptors. The quality and concentration of all sequencing libraries was assessed using a LabChip GX instrument (Perkin Elmer), followed by further quality control using a MiSeq sequencer (Illumina) to obtain optimal cluster densities, insert size and library diversities. Sequencing libraries (one sample per lane) were hybridized to the surface of HiSeqX flowcells (v2 or v2.5) using the Illumina cBot™. Paired-end sequencing-by-synthesis (SBS) was performed on Illumina HiSeqX sequencers, using 2x150 cycles of incorporation and imaging. Real-time analysis involved conversion of image data to base-calling in real-time. All steps in the sample preparation and sequencing workflow were monitored using an in-house laboratory information management system (LIMS) with barcode tracking of all samples and reagents.

Whole exome sequencing was performed as previously described in.[2] Following the standard procedures of sample preparation, we used the Agilent v7 exome kit, which has a condensed target size of 37 Mb focusing on pure coding regions. The design has been optimized with respect to bait selection and boosting based on empirical experience coming from the earlier versions to improve coverage evenness. Library preparation was performed with 200 ng of DNA using the SureSelectXT Automated Target Enrichment for the Illumina paired-end multiplexed sequencing protocol, and the Agilent Bravo automated liquid handling platform. After validation (2200 TapeStation; Agilent Technologies, Santa Clara, CA) and quantification (Qubit System; Invitrogen, Waltham, MA), pools of libraries were generated and subsequently sequenced on an Illumina HiSeq4000 sequencing instrument using a paired-end 2 × 75 bp protocol resulting in this case in an average coverage of 80x with 91% of the target region covered at least 30x. For data analysis, we used a new version of our Varbank analysis tool (Varbank 2.0) (https://varbank. ccg.uni-koeln.de/varbank2/), which refers to the GRCh38/hg38 reference human genome and provides a number of new features at the online graphical user interface.

**Culture and maintenance of probands-derived fibroblasts**

Primary human fibroblasts were cultured in DMEM (Dulbecco's Modified Eagle Medium) supplemented with 10% Fetal Bovine Serum (FBS, Biochrom), Penicillin/Streptomycin (Thermo Fisher Scientific), and Amphotericin B (Promocell). Cells were grown in 25cm or 75cm culture flasks and maintained in sterile incubators at 37°C, 95% relative humidity and 5% $CO_2$ atmosphere. All fibroblast lines were tested for mycoplasma contamination.

**Antibodies used in this study**

A detailed description of the antibodies used in this study (dilution, application, and manufacturer) is given in Table S1.

**Semi-quantitative reverse transcription PCR (RT-PCR)**

RNA was extracted from primary fibroblasts using the RNeasy kit (Qiagen), and concentrations were determined using the RiboGreen method (Life Technologies). 300ng of RNA were reverse transcribed to cDNA using the Quantitect Reverse Transcription Kit (Qiagen). Oligonucleotides were designed to flank *GBF1* exon 27 (FWD_Ex24_5′-CTACAGCGGGAAGAGACACC-3′ and REV_Ex28_5′-TGTGCCTGAACACAGAGGTG-3′) and exon 32 (FWD_Ex31_5′-GCTGTCCTTCATTGTGCGTG-3′ and REV_Ex33_5′-GAGGGTGCGAGAATCAGCTT-3′) in order to generate differently sized PCR products corresponding to potential alternate transcripts. PCR was performed with low cycle number (28) and 60°C annealing temperature).

**Western blot**

Probands-derived fibroblast were lysed in ice-cold RIPA buffer (SIGMA) with protease inhibitors (Complete Mini, Roche) for 30 minutes. After incubation, cells were centrifuged for 25 minutes, at maximum speed at 4°C. MNs were collected at the indicated time points (in vitro culture days DIV4, 12, and 20) and processed as described previously[4]. Dissected spinal cords and brains from P10 and P21 mice were snap-frozen and placed in homogenization tubes filled with ceramic beads (Peqlab). After the addition of ice-cold RIPA buffer with protease inhibitors, tissues were homogenized in the Precellys24 device (Peqlab) following a program of 25 seconds at 5500rpm. Immediately after, samples were sonicated for 10 minutes and centrifuged for 30 minutes at maximum speed at 4°C. If not immediately used, samples were stored at -80°C. Luminescent signal was detected using the detection reagents from Pierce™ ECL Western Blotting Substrate (Thermo Fisher Scientific) following the manufacturer´s instructions.

**Fibroblasts immunostaining**

40K cells grown on coverslips were washed three times with warm (37°C) PBS and fixed with 4% (w/v) paraformaldehyde (PFA). Fibroblasts were permeabilized in PBS-T (0.2% Tween-20) for 20 minutes and blocked for at least one hour in blocking solution (PBST + 5% BSA and 1% FCS). Primary antibodies were prepared in blocking solution and incubated overnight at 4°C. After three PBS-T changes, cells were incubated 1h at room temperature (RT) with different combinations of phalloidin and/or secondary antibodies diluted in blocking solution. After incubation, cells were washed three times with PBS-T and coverslips were rinsed in water prior mounting with ProLong mounting media with or without DAPI (Thermo Fisher Scientific). Information about antibodies and dilutions are given in Table S1.

**Experiments with murine-derived cells or organs**

All experiments involving mouse-derived cells and/or organs were approved by LANUV-NRW (Landesamt für Natur, Umwelt und Verbraucherschutz Nordrhein-Westfalen, reference number 84-02.04.2015.A378). Only wild-type (WT) FVB animals were used in this study.

**Generation and immunostaining of primary murine motor neurons**

For the generation of MNs, a pregnant mouse was euthanized and embryos at day 13.5 were removed from the uterus.[3] Embryos were sacrificed immediately by decapitation and the spinal cords were dissected as previously described[4]. Briefly, spinal cords were mechanically dissociated in 1% Trypsin (Worthington) with DNase I by pipetting. Isolated cells were seeded on Poly-D-Lysine (SIGMA) coated coverslips and grown in neuronal plating media consisting in DMEM supplemented with 5% Fetal Calf Serum (Biochrom), 0.6% Glucose (SIGMA).

Penicillin, Streptomycin, and amphotericin B. Cells were seeded in 12-well plates. 70K or 200K cells were seeded for imaging, or protein isolation, respectively. On the next day, the plating media was replaced for MN maintenance media consisting in Neurobasal medium (Thermo Fisher Scientific) supplemented with B27 (Thermo Fisher Scientific), 2 mM L-glutamine, Penicillin, Streptomycin, and Amphotericin B. In addition, the following growth factors were added: 50 ng/µl Ciliary Neurotrophic Factor (CNTF, Peprotech), 50 ng/µl Brain Derived Neurotrophic Factor (BDNF, Peprotech), and 50 ng/ul Glia Cell Line-derived Neurotrophic Factor (GDNF, Peprotech). MNs were maintained in sterile incubators at 37°C, 95% relative humidity and 5% $CO_2$ atmosphere. One-half of the culture media volume was refreshed every three days. 1µM Cytosine Arabinoside (AraC) was added to the media to eliminate dividing cells. MNs were fixed with 4% PFA supplemented with 4% sucrose (Sigma). Permeabilization, antibodies incubation, and mounting was performed as described for fibroblast immunostaining.

**Microscopy and image analyses**

Fluorescence images were acquired with a fully motorized microscope AxioImager M2 (Zeiss) equipped with an ApoTome.2 system mimicking confocality (Zeiss). NMJs images were acquired as z-stacks. Qualitative morphological analyses of Golgi morphology were based on GM130 staining. Precisely, the dispersion extent of the GM130 signal was categorized as: condensed or no fragmentation, intermediate fragmentation, and diffuse or extensive fragmentation. Golgi images were acquired with a 40X objective. More than 300 cells, representing three independent experimental replicates, were analyzed per fibroblast line. Fibroblast lines processing, image acquisition and quantification was performed blinded. For colocalization analysis, the Pearson colocalization coefficient was determined using the in-built colocalization tool of the ZEN software (Zeiss).

**Statistical analyses**

Statistical analyses were performed in GraphPad Prism 6 (GraphPad Software). Data are represented in percentage or as mean ± standard error of the mean/standard deviation (SEM/SD). Levels of statistical significance are given in GraphPad Prism 6 format where: * P = 0.05, ** P = 0.01, *** P = 0.001 and **** P = 0.0001. Specific statistical tests, sample size, and p values are indicated in the figure legends.

**SUPPLEMENTAL REFERENCES**

1. Karakaya, M., Storbeck, M., Strathmann, E.A., Delle Vedove, A., Holker, I., Altmueller, J., Naghiyeva, L., Schmitz-Steinkruger, L., Vezyroglou, K., Motameny, S., et al. (2018).

Targeted sequencing with expanded gene profile enables high diagnostic yield in non-5q-spinal muscular atrophies. Hum Mutat 39, 1284-1298.
2. Karakaya, M., Paketci, C., Altmueller, J., Thiele, H., Hoelker, I., Yis, U., and Wirth, B. (2019). Biallelic variant in AGTPBP1 causes infantile lower motor neuron degeneration and cerebellar atrophy. Am J Med Genet A 179, 1580-1584.
3. Hsieh-Li, H.M., Chang, J.G., Jong, Y.J., Wu, M.H., Wang, N.M., Tsai, C.H., and Li, H. (2000). A mouse model for spinal muscular atrophy. Nat Genet 24, 66-70.
4. Riessland, M., Kaczmarek, A., Schneider, S., Swoboda, K.J., Lohr, H., Bradler, C., Grysko, V., Dimitriadi, M., Hosseinibarkooie, S., Torres-Benito, L., et al. (2017). Neurocalcin Delta Suppression Protects against Spinal Muscular Atrophy in Humans and across Species by Restoring Impaired Endocytosis. Am J Hum Genet 100, 297-315.